Int. J. Solids Structures Vol. 25, No. 9, pp. 1023–1038, 1989
Printed in Great Britain.

0020–7683/89 $3.00 + .00
© 1989 Pergamon Press plc

THE APPLICATION OF A CONTINUUM DAMAGE MODEL IN THE FINITE ELEMENT SIMULATION OF THE PROGRESSIVE FAILURE AND LOCALIZATION OF DEFORMATION IN BRITTLE ROCK STRUCTURES

U. K. SINGH and P. J. DIGBY
Division of Rock Mechanics, Luleå University of Technology, S-951 87 Luleå, Sweden

(*Received* 16 *July* 1988; *in revised form* 2 *January* 1989)

Abstract—A continuum damage model is generalized to simulate both the progressive failure and the formation of localization bands in brittle rock structures under both tensile and compressive loading. The model is implemented into a finite element code to simulate the constitutive behaviour of a number of brittle rock structures which might actually be found in the laboratory or in the field.

1. INTRODUCTION

In an earlier paper [hereafter referred to as (I)], Singh and Digby (1989) developed a new continuum damage model to simulate the constitutive behaviour of brittle rocks loaded under plane strain conditions. To verify that physically satisfactory results could be obtained from the model before it was to be implemented into a finite element code, a number of idealized problems were first studied. The model was applied to predict the damage growth and constitutive behaviour of infinitely extended brittle solids loaded under plane strain conditions. Since only infinitely extended bodies were considered in (I), it could be supposed that the damage (due to the presence of cracks) in any given direction was uniformly distributed throughout the body. The effect of crack closure and friction in closed cracks could be included in the calculations performed in (I).

In the present paper, we extend the application of our damage model developed in (I). Thus, we now implement our model in a finite element code to study the damage growth and constitutive behaviour of a number of finitely extended bodies having different geometries and loaded under plane strain conditions. The effect of closed cracks will be included in the calculations. Since, in the present work, finitely extended bodies are considered, the damage in a given direction can no longer be supposed uniformly distributed throughout the body considered. Furthermore, in this case, the deformation of the body in the post-peak softening range can often be accompanied by a "localization" of the deformation into one or perhaps a number of discrete zones which traverse the body considered. In the present paper, we therefore also describe features which must be added to the model developed in (I) to simulate this behaviour.

2. LOCALIZATION OF DEFORMATION

We consider how the model developed in (I) may be extended to simulate the process of "localization of deformation" referred to in the Introduction of the present paper. All of the existing features of our model will be retained. A detailed description of these (together with the conventions adopted) has already been given in (I) and will not therefore be repeated here. We adopt the commonly accepted meaning of the term localization of deformation by saying that in the homogeneous deformation of an initially uniform material, non-uniform deformation may initiate and grow in one or several planar bands under continuing conditions of equilibrium and homogeneous deformation outside the band (see for example Rudnicki and Rice, 1975).

2.1. *Initiation of localization*

Rudnicki and Rice (1975) originally investigated this phenomenon theoretically by seeking conditions for which continued deformation (in an initially homogeneously deformed solid) would lead to a non-uniform field in which deformation rates could vary with position across planar (localization) bands but remain uniform outside these regions. If terms due to increments in the co-rotational stresses are neglected, Rudnicki and Rice (1975) then derived the following condition for initiation of a localization band with unit normal $\hat{\mathbf{x}}$:

$$\text{Det}\,(\alpha_i L_{ijkl} \alpha_l) = 0 \quad (i, j, k, l = 1, 2, 3) \tag{1}$$

In eqn (1), $\mathbf{L}$ is the tangential stiffness matrix, and components of $\hat{\mathbf{x}}$ and $\mathbf{L}$ are referred to a fixed set of rectangular Cartesian space axes. Components of the tangential stiffness matrix $\mathbf{L}$ are defined by the equations

$$\mathrm{d}\sigma_{ij} = L_{ijkl}\,\mathrm{d}\varepsilon_{kl} \tag{2}$$

The components of $\mathbf{L}$ possess the symmetries $L_{ijkl} = L_{jikl}$ and $L_{ijkl} = L_{ijlk}$ but for the constitutive model used in the present paper, $L_{ijkl} \neq L_{klij}$.

Unfortunately, in our numerical computations (to be described later) we found that it was very difficult to locate a state of deformation at which Rudnicki and Rice's conditions (1) and (2) are satisfied at each stage of the computations. We therefore attempted to use an alternative criterion in which the active damage planes are the only possible sites for the formation of localization bands within the structure considered. Thus, in the present paper, the orientations of the normals to all possible potential planar localization bands are first assumed to be coincident with those to the active damage planes [the procedure for determination of the orientation of the unit normal $\hat{\mathbf{x}}$ to an active damage plane has been fully explained in (1)]. We then supposed that localization could be initiated at points in the structure where under continuing deformation, the second-order work becomes zero or negative, that is,

$$\mathrm{d}\sigma_{ij}\,\mathrm{d}\varepsilon_{ij} \leqslant 0 \tag{3}$$

for given admissible strain increment components $\mathrm{d}\varepsilon_{ij}$ (again referred to space axes).

2.2. *Post-peak load–deformation behaviour*

After the localization of deformation in a structure, if we continue loading then loading also continues in the localized band but zones outside the band will continue to unload. In other words, the deformation in the localized band increases while other regions in the structure relax. In this process, the unloading regions of the structure release a quantity of strain energy given by

$$W_u = \int_{\text{Volume of the unloading part}} (\boldsymbol{\sigma} \cdot \mathrm{d}\boldsymbol{\varepsilon})\,\mathrm{d}V \tag{4}$$

and the energy supplied to the localized band is given by

$$W_l = \int_{\text{Volume of the localized band}} (\boldsymbol{\sigma} \cdot \mathrm{d}\boldsymbol{\varepsilon})\,\mathrm{d}V \tag{5}$$

for continued loading. Equations (4) and (5) are valid for admissible strains. When the magnitude of the energy released is less than the energy supplied (required), i.e.

$$|w_u| < |w_l|, \tag{6}$$

in the structure, then it is stable under displacement-controlled loading. In other words, the load in the structure decreases with increasing deformation. This behaviour is called "snap-through" load–deformation behaviour (curve ad in Fig. 1). If the condition

$$|w_u| > |w_l| \tag{7}$$

is satisfied, then the structure is unstable even under displacement-controlled loading. Here, a quantity of excess unloading energy

$$w_a = |w_u| - |w_l| \tag{8}$$

is available for loading the localized zone at a constant, specified deformation of the structure (see Fig. 1). An excess of energy w_a is available for dynamic loading of this localized band. Unfortunately, dynamic behaviour cannot be simulated in a static analysis.

To circumvent this problem, one may consider the excess unloading energy w_a by artificially unloading the structure. The energy w_a is then not available for loading the localized band. In this way one avoids the dynamic situation. This type of load–deformation behaviour is called "snap-back". This is shown by curve abc in Fig. 1. The shaded area in the figure denotes the excess unloading energy. If the deformation at point a is maintained constant, then the load drops suddenly from a to c without any significant overall deformation. The actual load–deformation path followed is abc which is of the snap-back type. From Fig. 1 we also see that if one is not interested in the details of the equilibrium path abc, when condition (7) is satisfied, then in displacement-controlled loading considered in this work, equilibrium of the structure may still be restored at point c.

The localized band is usually narrow and its width is almost independent of the size of the structure. For example, in earthquake faulting, landslide and foundation failure, most of the deformation is localized in a concentrated, narrow zone whose width is almost independent of the volume of the rock mass involved in the process. Hence as indicated above, the flux of energy (from that part of the structure outside the band) into a fixed, given volume of localization band increases with the size of structure. Thus the load–deformation behaviour in the post-peak softening range (i.e. after localization) appears to depend on the size of the structure. The deformation in the band increases with w_u. The stress is a fixed function of strain given for example by the constitutive relation (9) in (I). Hence, the larger the size of the structure, the greater will be the decrease in the overall load for a given increment in overall deformation.

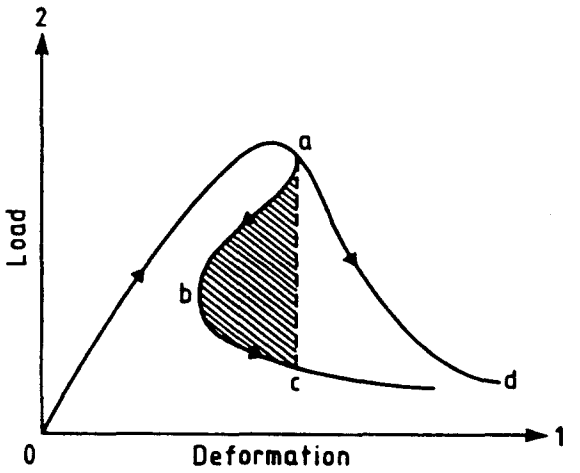

Fig. 1. Load–deformation behaviour of a structure. The shaded region shows excess unloading energy in the post-peak strain softening range.

2.3. *Constitutive model used for an element in which localization has been initiated*

For all elements in which condition (3) is not satisfied, all details of damage growth are simulated by our continuum damage model (I) in its original form. For those elements in which condition (3) for localization of deformation is satisfied, however, our constitutive model (I) must be generalized. Thus, once condition (3) for localization of deformation within a given element is satisfied, then the strain field within this element will no longer be uniform. Here, a planar localization band of thickness b^l, say, will be formed. In our computations, the minimum element length, b, say, will always be larger than the band width b^l, and b^l is also taken to be a fixed, characteristic property of the material considered. As mentioned earlier, active damage planes, whose normals $\hat{x}$ have known orientations [from our earlier work (I)], are assumed to be the only possible sites for the formation of localization bands. Now after inequality (3) is satisfied, that is, localization within this element has been initiated, we suppose that any further softening (due to further damage growth) will occur only within the localization band. The other part of this element (outside the band), we suppose, now unloads elastically. Thus, under further loading of the element, the compliance of that part of the element outside the band remains constant and equal to its value at the initiation of localization.

From the finite element analysis, we can calculate the average strain components ε_{ij} in the localized element considered by using the nodal displacements of the element. We calculate ε_{ij} at the center of the element. Let C_{ijkl}, $C^{(e)}_{ijkl}$, $C^{(l)}_{ijkl}$, $(i, j, k, l = 1, 2, 3)$ be the components (all referred to space axes) of the compliance tensors for the element, the elastically unloading part of the element, and the localized band, respectively. The effective compliance of the element may be calculated assuming that the stress is homogeneous throughout the localized element, that is, in particular,

$$\sigma_{ij} = \sigma^{(l)}_{ij}. \tag{9}$$

We also have in this case,

$$C_{ijkl} = \left(1 - \frac{b^l}{b}\right) C^{(e)}_{ijkl} + \frac{b^l}{b} C^{(l)}_{ijkl}. \tag{10}$$

It follows from eqn (10) that for $b^l = b$, when the localized band includes the complete element, the effective compliance of the element will be equal to that of the localized band. The effective stress in the element is given by

$$\sigma_{ij} = (C)^{-1}_{ijkl} \varepsilon_{kl}. \tag{11}$$

The stress within the localized band is

$$\sigma^{(l)}_{ij} = (C^{(l)})^{-1}_{ijkl} \varepsilon^{(l)}_{kl} \tag{12}$$

where $\varepsilon^{(l)}_{ij}$ and $\sigma^{(l)}_{ij}$ denote the components of strain and stress tensor within the localized band, calculated by using the constitutive relation

$$\sigma^{(l)}_{ij} = K_{ijkl}(D) \varepsilon^{(l)}_{kl} \quad (i, j, k, l = 1, 2, 3) \tag{13}$$

[eqn (9) in (I)]. Now, using the above assumption of homogeneity of stress within the element [eqn (9) above] together with eqns (11) and (12) we find that

$$\varepsilon^{(l)}_{ij} = C^{(l)}_{ijpq} (C)^{-1}_{pqrs} \varepsilon_{rs} \tag{14}$$

(the superscript "-1" in eqns (11), (12) and (14) above denotes matrix inversion). We use the strain within the localization band, calculated from eqns (14) in the constitutive equation (13) which describes the softening behaviour of the material within the band. This model of localization can now be included in our original constitutive model (I).

2.4. *Dependence of computational results obtained on finite element mesh size. Restriction on mesh size*

As indicated in Sections 2.2 and 2.3 of this paper, whenever localization of deformation is generated within one or several bands in a brittle rock structure, the results of a finite element analysis will depend on the size of the element used in the discretization. Some kind of element size control technique must then be developed to overcome this difficulty. In Bazant's work (1986), the fracture energy dissipated will be independent of the element length h for any value of $h \geq h'$, where h' is the crack band width in Bazant's strain softening crack band model. However, Bazant (1986) imposed the additional restriction that the element length h should also satisfy the inequality $h < 3h'$. It was then found that snap-back behaviour (see our discussion in Section 2.2) at the element level could be avoided. Our approach is similar in principle to Bazant's. However, our method is motivated by the observation that in the post-peak strain softening range, the deformation is localized to a narrow band whose width h' is independent of the size of structure considered. In our method, the strain in the band is calculated from eqn (14) given the element length and band width. This calculated strain is then used in the constitutive relation. The element length used in the region of localization in our model is also restricted to lie in the range $h' \leqslant h < 3h'$.

A strain gradient approach has also been developed by Schreyer and Chen (1986) in which finite elements smaller than the width of the localized band may be used. Here the strain gradient calculated over the elements will determine the number of the elements to be included in the band. However the strain gradient cannot be calculated in the displacement formulated finite element analysis used in our work.

3. FINITE ELEMENT SIMULATION OF THE CONSTITUTIVE BEHAVIOUR OF FINITELY EXTENDED BRITTLE SOLIDS LOADED UNDER PLANE STRAIN CONDITIONS

The constitutive model developed both in (I) and also in this paper has been implemented into the finite element code NFEMP. NFEMP is a non-linear version of the finite element code FEMP developed by Nilsson and Oldenburg (1983). In all of the problems studied in this section, the body considered is loaded under plane strain conditions. The numerical values of the appropriate material parameters [see (I)] are listed in Table 1. These are used in all of the problems studied in this section. They were obtained from uniaxial tension and simple shear tests on samples of a grey, medium grained granite from the Stripa mine in central Sweden (see Shahidi *et al.*, 1986, for further details). We denote the applied boundary loading parameter by "time" and axes 01 and 02 by X and Y, respectively. The arrow marks at both ends of line segments in the principal stress and strain plots (for example in Figs 3a and 3b) denote tensile components. Line segments with arrow marks omitted denote compressive components. Arrow marks at both ends of line segments in damage plane plots (for example in Fig. 3c) denote actual (growing) damage (crack) planes. In displacement vector plots (for example in Fig. 3d), arrows denote the directions of displacements. The length of line segments in all the plots shown is proportional to the magnitude of the quantity plotted.

Table 1. Numerical values of the constitutive parameters used in the finite element simulations

Parameter	Value
E	30.0×10^9
ν	0.2
σ_{N_c}	-0.5×10^6
A_1	312.5
A_2	1.15×10^{-3}
A_3	0.20×10^{-3}
D_0	1.0×10^{-5}

Modified damage growth law given by eqns (24a) and (24b) in (I).

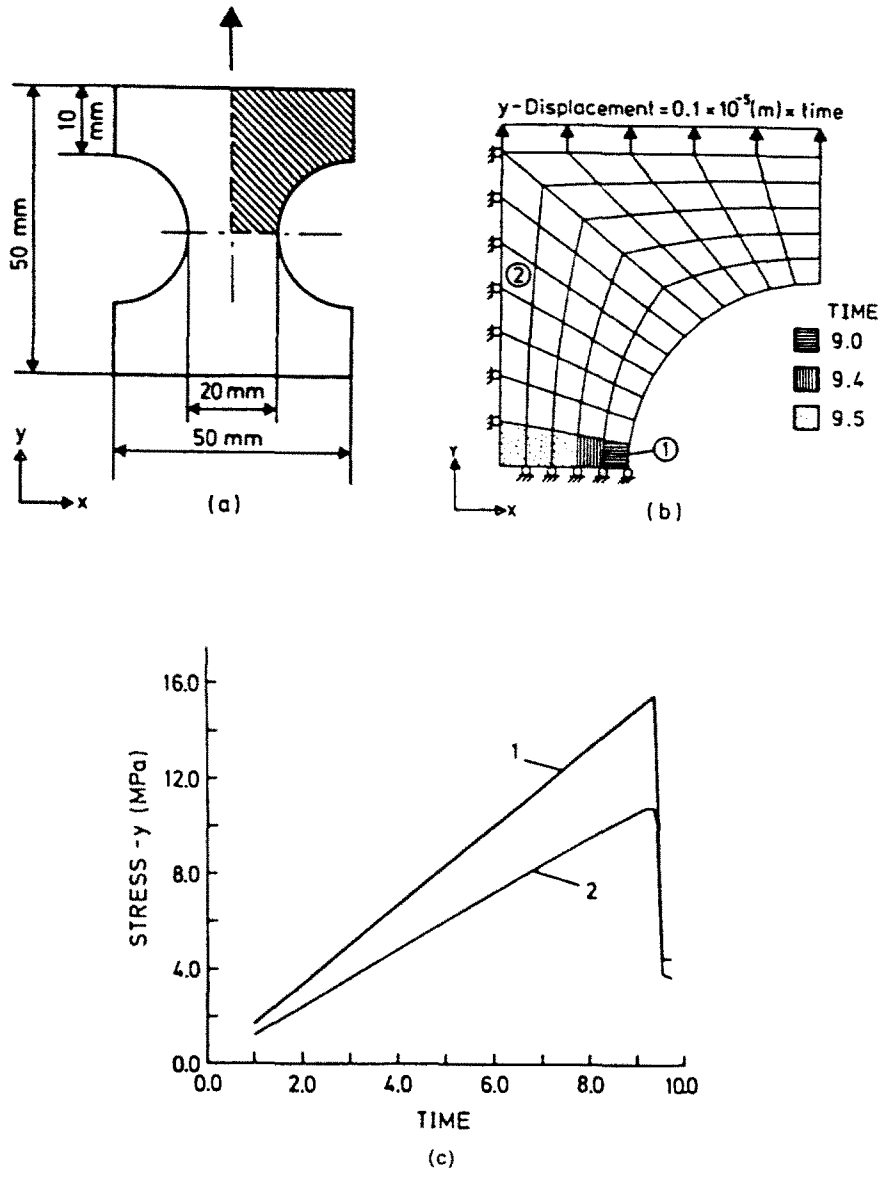

Fig. 2. (a) Specimen geometry and loading direction for the problem in Section 3.1. (b) Finite element discretization and boundary conditions of the shaded area in (a). Shaded elements are elements in which localization has occurred at different times. (c) Y-stress vs time graphs for the problem in Section 3.1. Curve (1) is for the element at point (1) and curve (2) is for the element at point (2) shown in Fig. 2b.

3.1. *A specimen loaded under tension*

The specimen geometry, boundary conditions and finite element discretization are shown in Figs 2a and 2b. The specimen is loaded under displacement-controlled conditions by specifying the displacement $= 0.1 \times 10^{-5}$ (m) $\times$ time in the Y-direction, at the top of the specimen as shown in Fig. 2b. We have used a time increment equal to 1 from time 0 to 8 and equal to 0.1 onwards. A characteristic localization band width (characteristic length) of 2 mm has been used in this analysis.

The graph of Y-stress vs time for points (1) and (2) (Fig. 2b) is shown in Fig. 2c. The results at time 9 are shown in Figs 3. At time 9 one element, shown in Fig. 2b, becomes localized. Here, a sudden drop in stress (load) occurs at time 9.4 for a time increment 0.1. Results at time 9.5 are shown in Figs 4.

In Figs 3, we observe that damages (cracks) initiate in regions of stress and strain

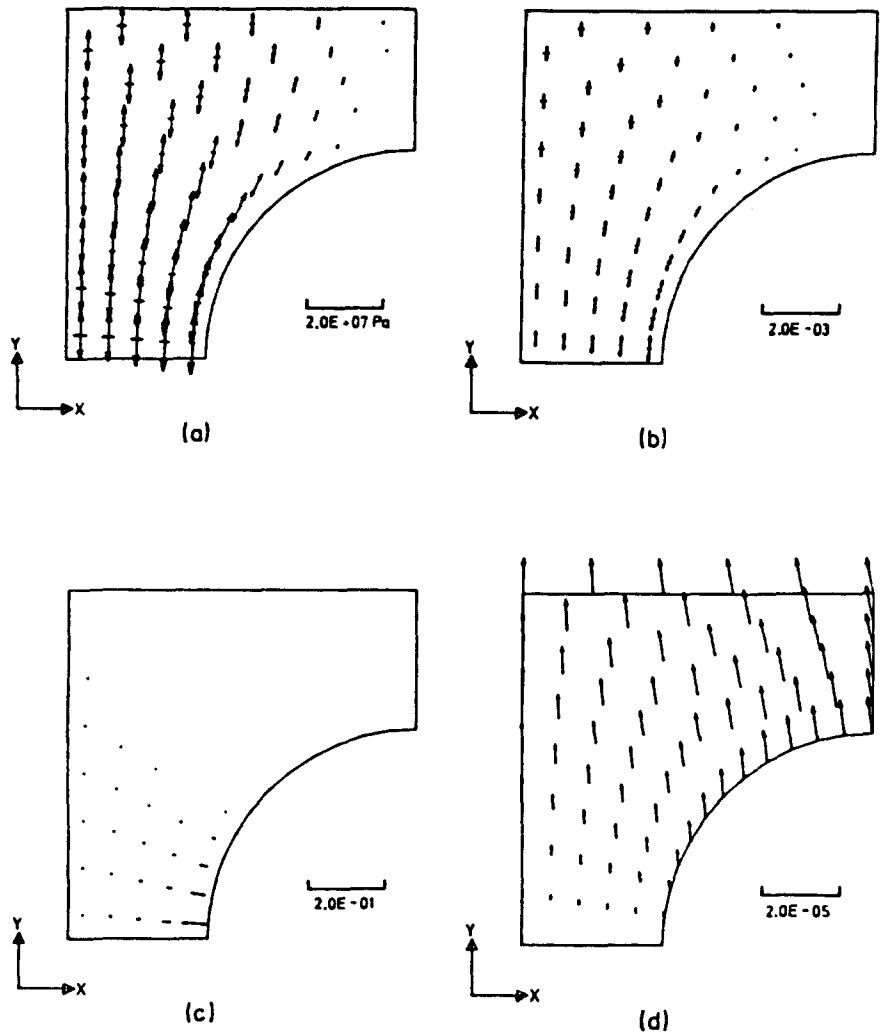

Fig. 3. Results at time 9 for the problem in Section 3.1. (a) Principal stress components; (b) principal strain components; (c) damage planes; (d) displacement vectors.

concentration, and the damage planes are normal to the maximum principal stress and strain directions. At time 9, one element localizes (softens) (cf. Fig. 2b) while the specimen bears increasing loads (Fig. 2c). With an increase in applied load, more elements localize, and after the peak applied load is reached, these localized elements form a band of softening elements (Fig. 2b), which we call a localization band. The principal strain plots at time 9.5 (Fig. 4b), after the formation of the localization band, indicate the presence of large deformations (strain) in the band and comparatively small deformations (strain) outside this band. The largest magnitude of the damage occurs within the localization band (Fig. 4c). That part of the specimen outside the band appears to translate as a rigid body (Fig. 4d). A sharp drop in load after the peak, shown in Fig. 2c, reveals that the post-peak behaviour of the specimen is of the snap-back type described in Section 2.2), i.e. unstable under displacement control in the post-peak region. A similar type of instability has been observed in direct tension tests on granite and sandstone specimens in the laboratory by Shahidi *et al.* (1986).

3.2. *Simulation of shear band formation under applied compressive loading*

The specimen geometry boundary conditions and finite element discretization for the problem described here are shown in Fig. 5. To initiate localization in the homogeneously strained specimen, we introduce some initial finite damage within the four shaded elements shown in Fig. 5. The specimen is loaded under displacement-controlled conditions by

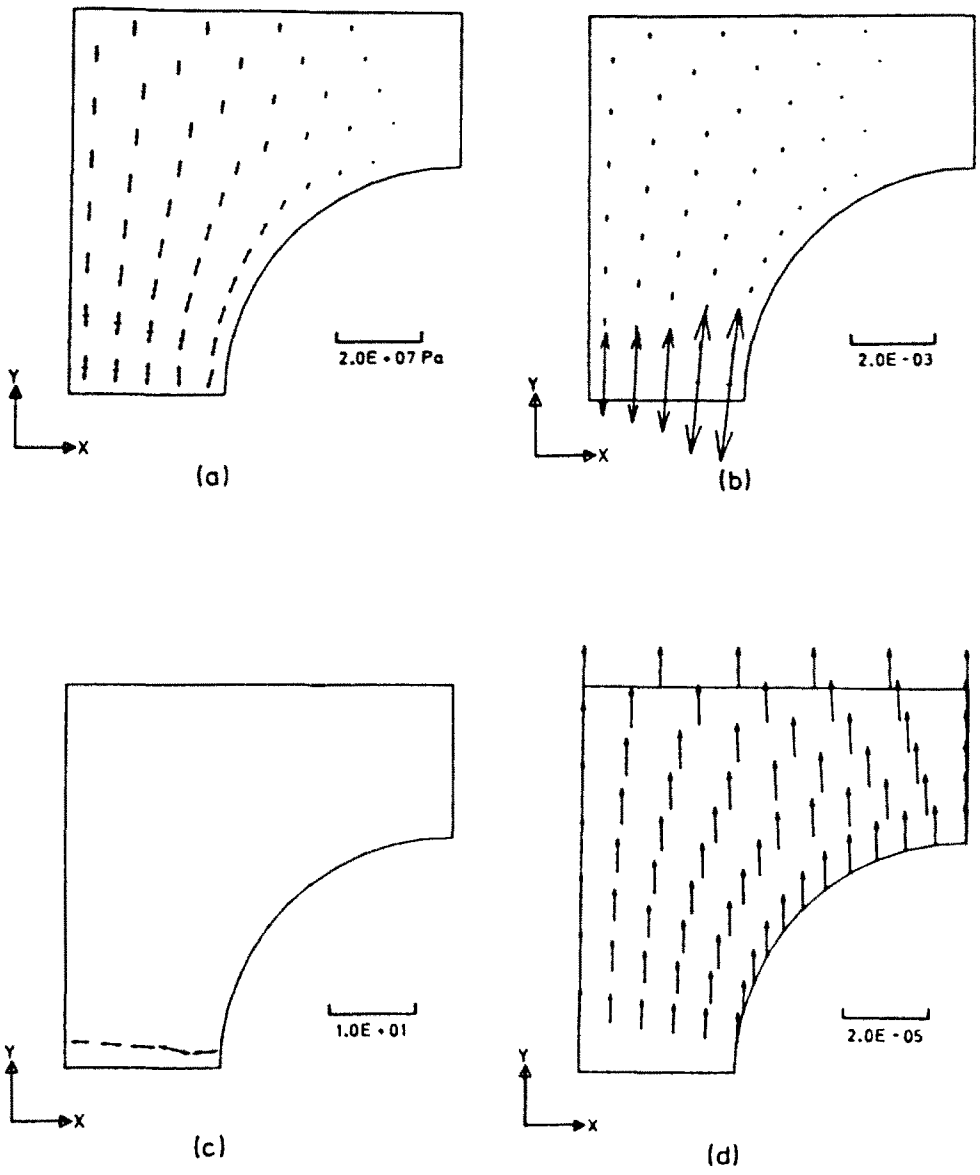

Fig. 4. Results at time 9.5 for the problems in Section 3.1. (a) Principal stress components; (b) principal strain components; (c) damage planes; (d) displacement vectors.

specifying a displacement $= -0.1 \times 10^{-4}$ (m) $\times$ time in the Y-direction at the top of the specimen. We have used smaller time increments near the peak load.

The graph of Y-stress vs time at point (1) (Fig. 5) is shown in Fig. 6. Some results at time 25.6, after which time a few elements have localized, are shown in Figs 7. As in the tension experiment described in Section 3.1, we observe that from time 25.5 to 26.2 an increasing number of elements localize, as indicated in Figs 8, while the specimen carries an increasingly large load (Fig. 6). At time 26.2, the peak load is reached. At the next time increment, the localizing elements join to form a localized band (Figs 9). The results in the post-peak region, at time 26.3, are shown in Figs 9. Unlike the tension loading described in Section 3.1, the localized band consists of a band whose thickness is approximately four elements (Figs 9b,c,f), and the damage planes are approximately normal to the localization band (Fig. 9e). Cracks of this type associated with relative shear displacements have been observed by Shahidi *et al.* (1986) in direct shear tests on intact Stripa granite specimens. These damage planes may be compared with observed en-echelon fissures associated with faulting (Dennis, 1972, p. 302).

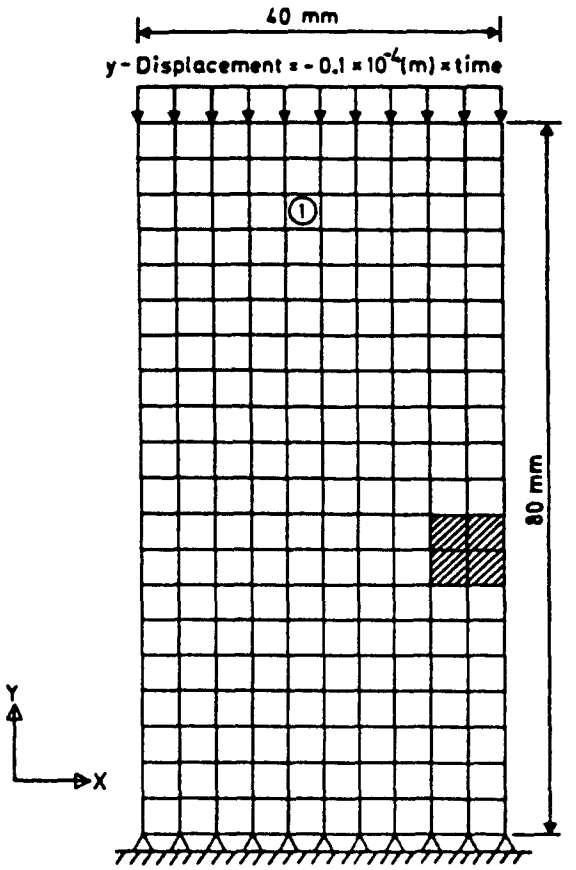

Fig. 5. Specimen geometry, boundary conditions and FE discretization for shear band simulation under compressive loading. Shaded elements have an initial damage of 0.5 with the normal to the damage plane at an angle of 170° to the X axis.

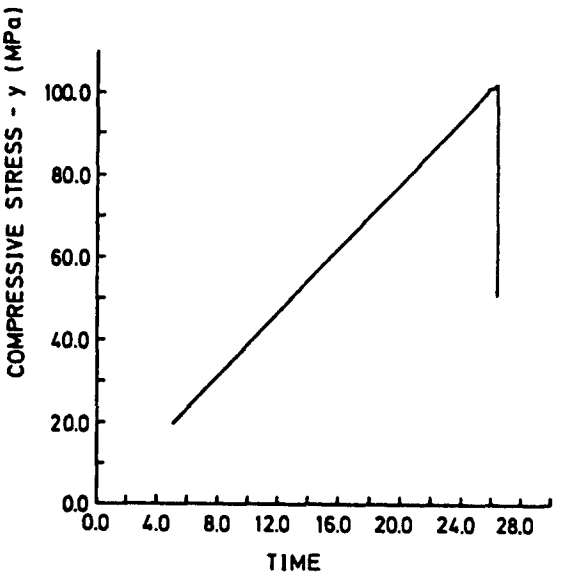

Fig. 6. Stress-Y vs time graph for the element at point (1) in Fig. 5.

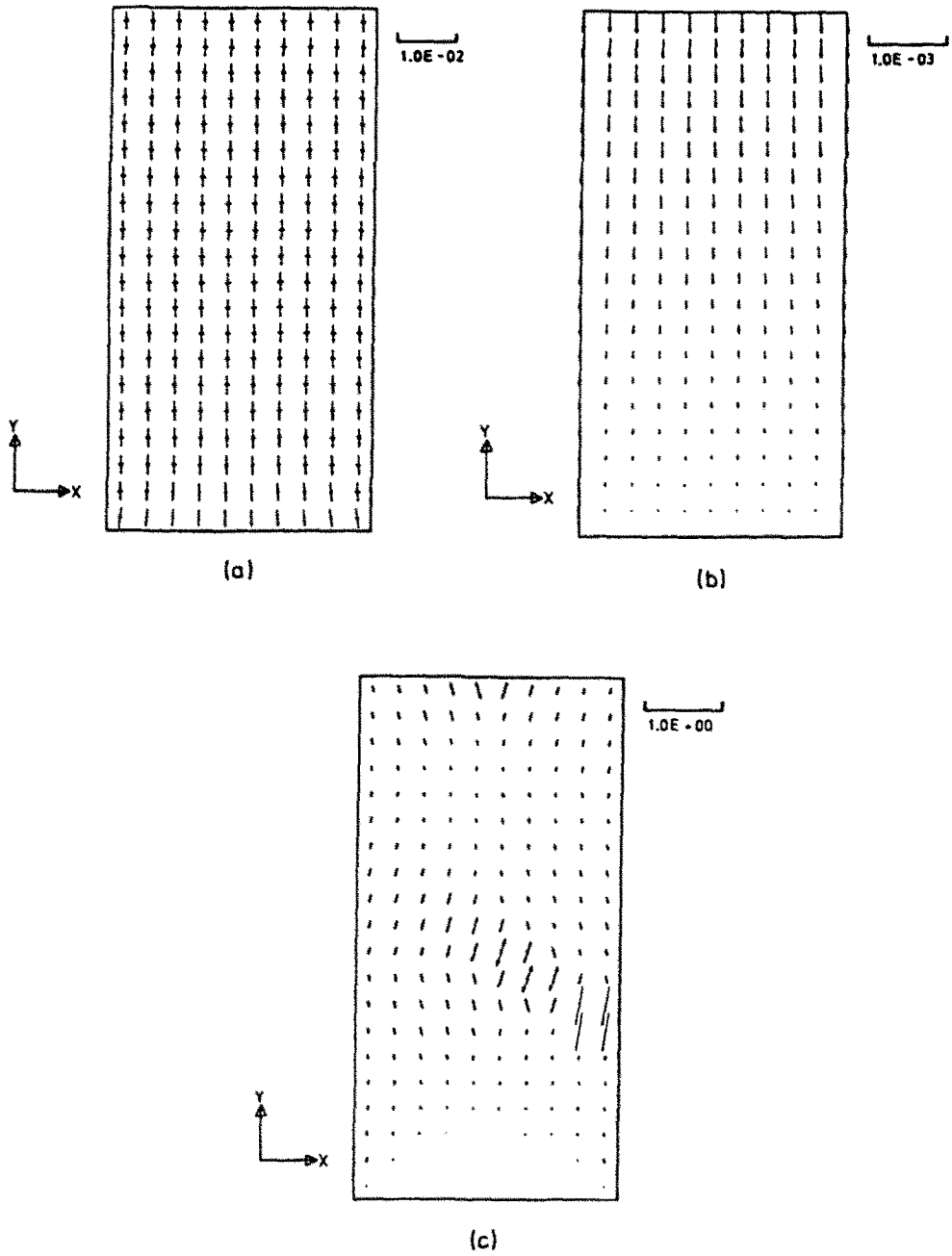

Fig. 7. Results at time 25.6 for the problem in Section 3.2. (a) Principal strain components; (b) displacement vectors; (c) damage planes.

3.3. *Failure around a rectangular tunnel excavated in a brittle rock*

Figure 10 shows a cross-sectional view of a rectangular tunnel, together with the geometry, boundary conditions and FE discretization of the tunnel. We loaded the tunnel by applying a vertical compressive load (in the Y-direction) equal to -1.0 (MN m^{-2}) $\times$ time. This is equivalent to a Y-stress of -1.0 (MPa) $\times$ time at a point in the rock mass remote from the tunnel. We do not consider gravitational loading in this case. We have used time increment 9 up to time 54, and 1 afterwards. At time 54, a few elements begin to localize (Fig. 11). In these elements the X-stress and strain are tensile. The localization in these elements (shown in Fig. 12d) is therefore of the type described in Section 3.1 for the case of tensile loading. As time increases, more elements gradually localize in the compressive stress field around the tunnel as shown in Fig. 11. The results at time 57 are shown in Figs

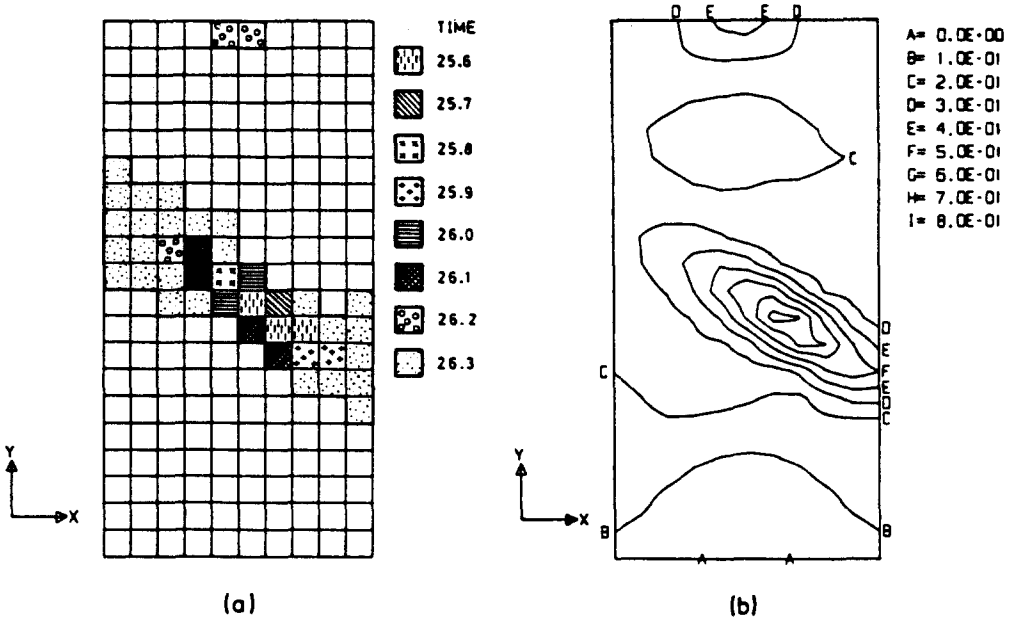

Fig. 8. (a) Localized elements at different times for the problem in Section 3.2; (b) damage contours at time 25.9.

12 and those at time 59, after which time we could not continue the numerical loading, are shown in Figs 13. The stresses and strains in the elements at points (1), (2) and (3) (Fig. 10) have been monitored continuously. We observed a peak Y-stress of -114.0 MPa in the element at point (3) at time 58. The Y-stress at that point dropped to -46.8 MPa at time 59. The stresses at point (1), remote from the tunnel opening, continued to increase. However, comparing Figs 12c and 13c, we observe that a part of the region immediately surrounding the localization zone unloads.

This results in the snap-back type of instability (discussed in Section 2.1) at the tunnel wall. Violent failure of a rock mass in a tunnel due to large induced stresses results from this type of instability (Jaeger and Cook, 1979). Comparing the stress plots at times 57

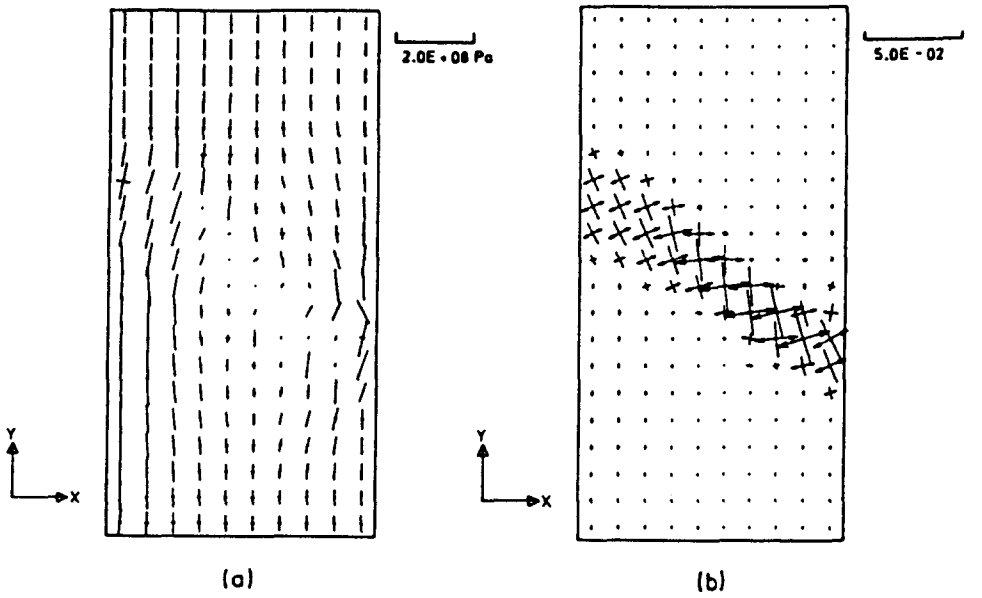

Fig. 9. Results at time 26.3 for the problem in Section 3.2. (a) Principal stress components; (b) principal strain components; (c) deformed and undeformed specimen; (d) displacement vectors; (e) damage planes; (f) damage contours.

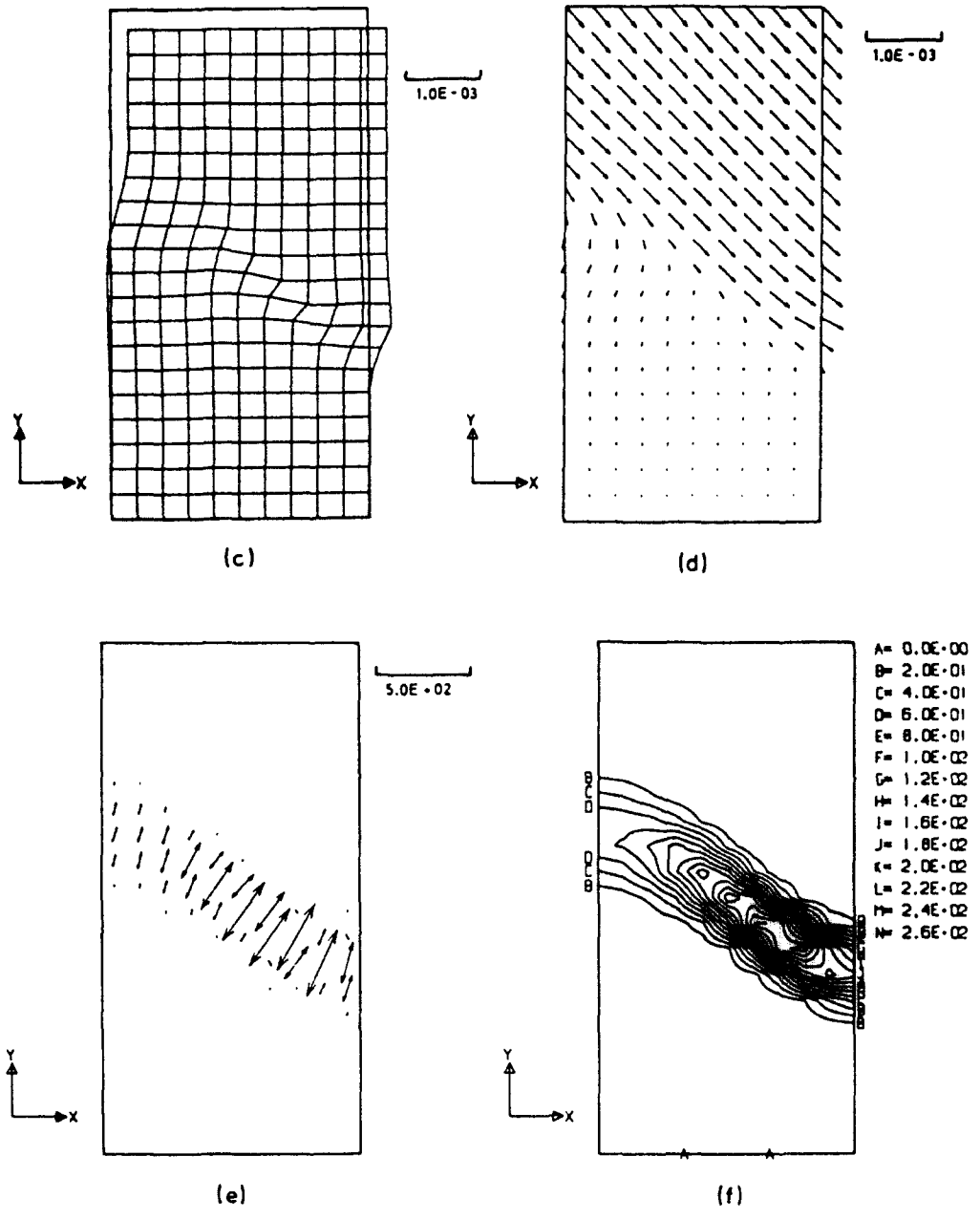

Fig. 9—*continued.*

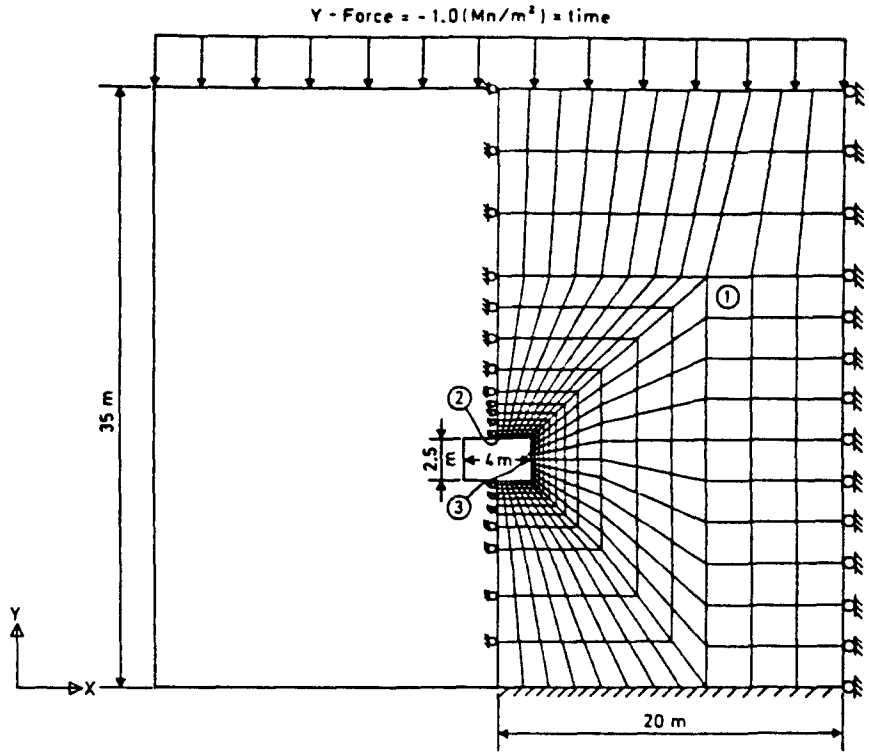

Fig. 10. Boundary conditions and FE discretization for the failure analysis around a rectangular tunnel (cross-sectional view of the tunnel).

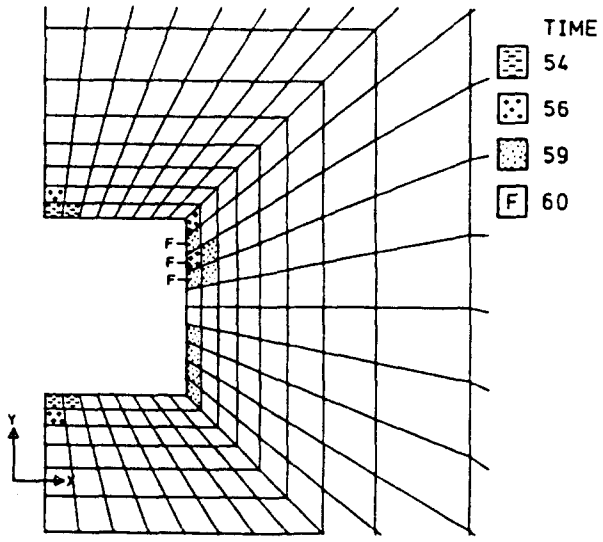

Fig. 11. Localized and completely failed elements at different times for the problem in Section 3.3.

(Figs 12a,b) and (Figs 13a,b), we observe that the region of stress concentration moves into the rock mass from the tunnel wall as the rock fails. Contour plots of the damage at time 59 in Figs 13e,f show the extent of damage around the tunnel.

We were unable to continue loading of the tunnel beyond time 59, since in a few elements (marked 'F' in Fig. 11) the magnitude of the damage had reached a very large value. This resulted in "ill-conditioning", i.e. an almost singular behaviour of the overall effective elastic compliance matrix of the material in those elements.

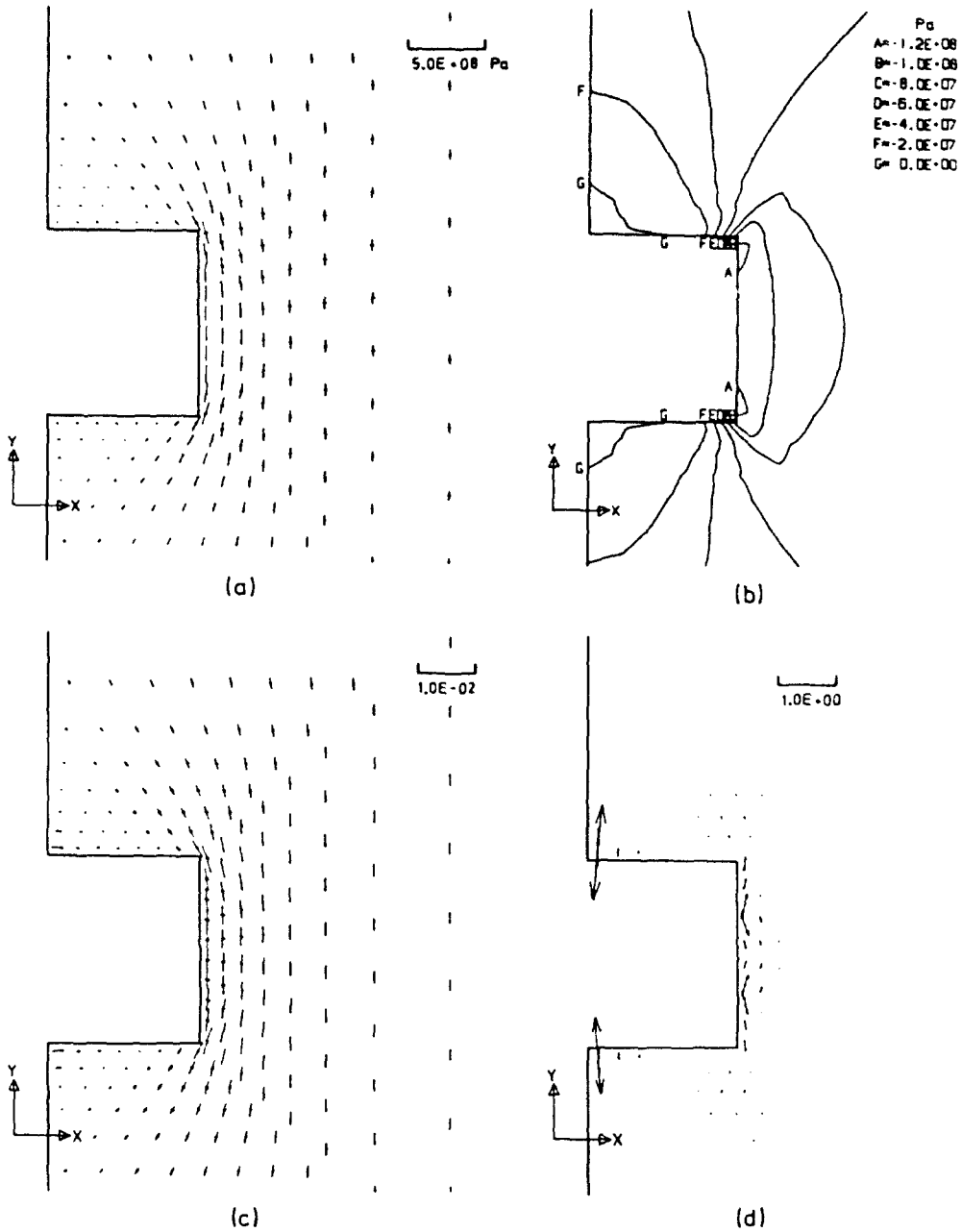

Fig. 12. Results at time 57 for the problem in Section 3.3. (a) Principal stress components; (b) stress-Y contours; (c) principal strain components; (d) damage planes.

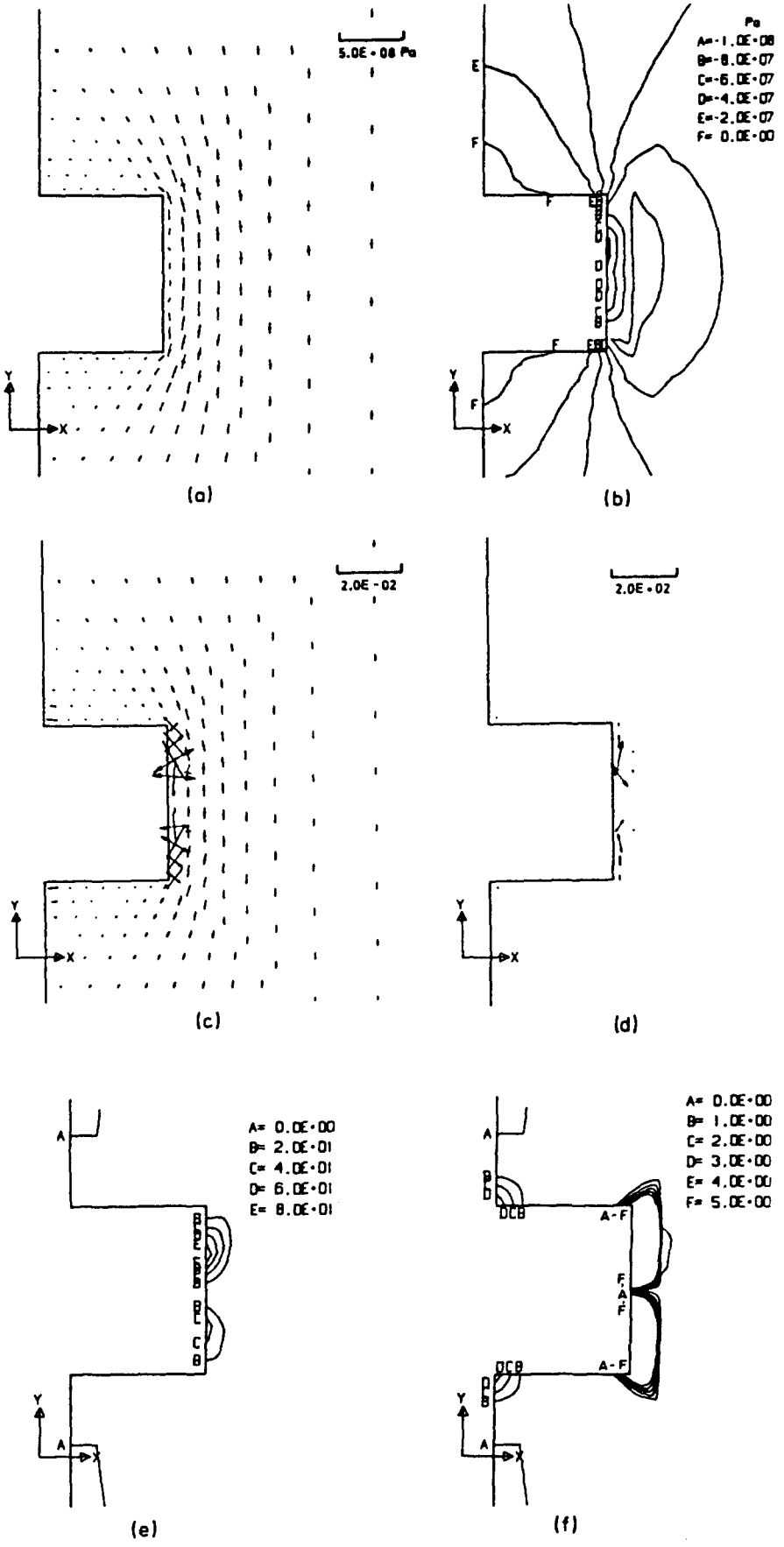

Fig. 13. Results at time 59 for the problem in Section 3.3. (a) Principal stress components; (b) stress-Y contours; (c) principal strain components; (d) damage planes; (e) damage magnitude contours, 0–80; (f) damage magnitude contours, 0–5.

4. DISCUSSION

In the present paper, we have implemented our constitutive model developed in (I) into a finite element code to simulate the progressive failure of brittle rock structures loaded under plane strain conditions. The structures considered resemble those which might actually be encountered in the laboratory or in the field. Our constitutive model originally developed in (I) can now also be used to simulate the formation of localization bands in brittle rock structures under both tensile and compressive loading. From the numerical simulations performed it will be noticed, as in (I), that a series of material parameter "sensitivity" studies for a range of cracked materials under given loading conditions was not performed. Once again, we believe that equally large or even far greater contrasts in the constitutive behaviour may be observed by studying a given cracked solid subjected to different applied loading conditions. It will also be noted that we have been unable to resolve completely the problem of dependence of our computational results on the mesh size. This must await further work. Nevertheless, we do believe that our constitutive model simulates many of the essential observed features of progressive failure in brittle rock structures at least in a qualitatively correct manner.

Acknowledgements—Financial support for this work was provided by Luleå University of Technology and STU (National Swedish Board for Technical Development), Grant no. STU85:3997. The drawings were prepared by Mrs Monica Leijon. We would also like to thank Professor Ove Stephansson (Division of Rock Mechanics, Luleå University of Technology) for his encouragement during the course of this work.

REFERENCES

Bazant, Z. P. (1986). Mechanics of distributed cracking. *Appl. Mech. Rev.* **39**, 675.

Dennis, J. G. (1972). *Structural Geology*. John Wiley and Sons, New York.

Jaeger, J. C. and Cook, N. G. W. (1979). *Fundamentals of Rock Mechanics*, 3rd edn. Chapman and Hall, London.

Nilsson, L. and Oldenburg, M. (1983). FEMP—An interactive graphic finite element program for small and large computer system. Technical Reports 1983:07 T and 1983:08 T, Luleå University, Luleå, Sweden.

Rudnicki, J. W. and Rice, J. R. (1975). Conditions for the localization of deformation in pressure-sensitive dilatant materials. *J. Mech. Phys. Solids* **23**, 371.

Schreyer, H. L. and Chen, Z. (1986). One dimensional softening with localization. *J. Appl. Mech.* **53**, 791.

Shahidi, P., Stephansson, O. and Singh, U. K. (1986). Control of uniaxial tension and simple shear test after peak-load. Research Report TULEA 1986:15, Luleå University, Sweden.

Singh, U. K. and Digby, P. J. (1989). A continuum damage model for simulation of the progressive failure of brittle rocks. *Int. J. Solids Structures* **25**, 647–663.